JOURNAL OF MATERIALS SCIENCE 27 (1992) 3969–3976

Measurement and analysis of the fracture of a liquid crystal polymer

J. SWEENEY, B. BREW, R. A. DUCKETT, I. M. WARD
IRC in Polymer Science and Technology, University of Leeds, Leeds LS2 9JT, UK

The fracture initiation behaviour of injection-moulded plaques of a liquid-crystal polymer is described. Attention is restricted to cracks in the plane of the plaques propagating along the mould fill direction. The material is both anisotropic and inhomogeneous; the latter factor is accommodated by adopting a skin–core model of the plaque structure. The inhomogeneity leads to mixed mode (Modes I and II) fracture in some cases, and both single and mixed-mode testing is used. The results can be represented in terms of either stress intensity or strain energy release rate by simple mixed-mode failure criteria.

1. Introduction

Although the structure and properties of thermotropic liquid-crystalline polymers have been the subject of a number of investigations [1–6], their fracture behaviour has been less extensively studied, in spite of their potential interest as engineering materials. A major complication occurs in these polymers when they are melt processed due to the fact that the molecular orientation depends locally on flow fields which vary from point to point. In this paper we describe fracture toughness measurements on injection-moulded plaques where the mechanical anisotropy varies substantially across the section.

The approach adopted is influenced by the recognition that inhomogeneous material leads inevitably to mixed-mode crack-tip conditions, and so the behaviour under combined Mode I and Mode II loading must be studied. We have carried out both single mode and mixed mode tests and have used finite-element modelling to assist in their interpretation. In the case of the mixed-mode tests, techniques were employed in association with the finite-element analyses to separate the Mode I and II contributions. The results are discussed in terms of mixed-mode failure criteria.

2. Experimental procedure

2.1. Materials

The material, a development polymer manufactured by ICI, was based on a copolyester comprising *p*-hydroxybenzoic acid (HBA)/isophthalic acid (IA)/hydroquinone (HQ) in the proportions 36(HBA):32(IA):32(HQ). It was supplied in the form of picture-frame mouldings of thickness 6 mm and otherwise as defined in Fig. 1. A detailed description of the structure and mechanical properties of the mouldings is given in a separate publication [7].

This study is confined to material in the rectangular region ABCD of Fig. 1. Because the mouldings are made by injection at a single gate, at Point I in Fig. 1,

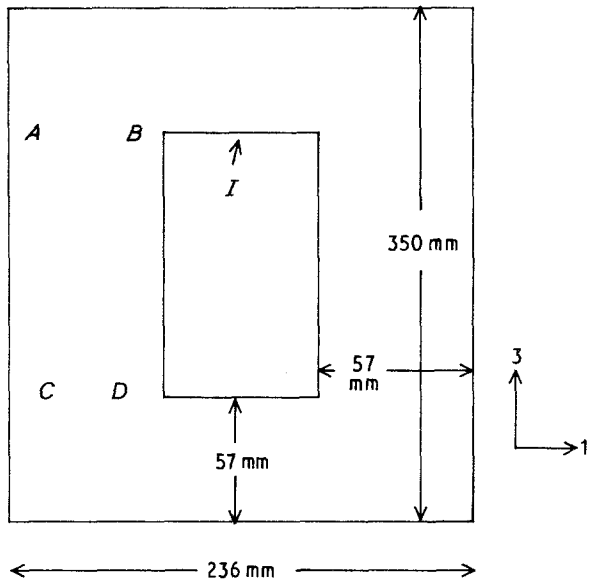

Figure 1 Picture frame plaque. Injection point is at I.

the flow in this region is approximately laminar. We would, therefore, expect the resulting material to be sensibly orthotropic with the 3-axis (as defined in Fig. 1) along the principal direction associated with the highest stiffness. The inhomogeneity can be approximated by a laminar structure consisting of layers in the plane of the moulding. The mechanical properties of this region of the material were measured previously [7] as a function of position within the moulding thickness (along the 2 direction) using techniques involving the removal of thin plane layers of this form. The profile of properties was seen to vary from plaque to plaque and within the same moulding, but in all cases there were found to be stiff layers of relatively high orientation at the surfaces to a depth of ~ 0.3 mm of the 6 mm thickness. A skin–core model, therefore, retains the reproducible features of the structure, and this model is adopted for the present work. The mechanical properties of the skin and core

TABLE I Compliances

	Compliance (GPa^{-1})							
	s_{11}	s_{22}	s_{33}	s_{12}	s_{23}	s_{31}	$s_{44} = s_{55}$	s_{66}
Skin	0.50	0.46	0.063	− 0.35	− 0.051	− 0.029	1.04	1.81
Core	0.50	0.46	0.12	− 0.35	− 0.051	− 0.056	1.04	1.81

materials, obtained from the average properties measured in [7], are given in Table I, where the 1- and 3-axes are as defined in Fig. 1, and the 2-axis is normal to the plane of the plaque.

2.2. Testing

All the tests were designed to cause cracks to grow along the 3 direction in the plane of the moulding. Cracks propagate most readily in this plane and so this form of test is of most practical relevance. Specimens were aligned with their axes along the 3 direction and were of width 10 mm in the 1 direction; a typical arrangement of the original specimen locations within a plaque is shown in Fig. 2.

There were three basic classes of experiment; Mode I, Mode II and mixed mode. All three forms of test are illustrated in Fig. 3. The Mode I tests were of the double cantilever beam type, with the tensile load applied to the specimen via hinges glued to its surfaces as shown in Fig. 3a. In the other two forms of test, the load is applied via a four-point bend system. In the Mode II test of Fig. 3b the crack grows in the central plane of the specimen. In the mixed mode specimen of Fig. 3c the crack grows from a notch originating at the corner of a step machined in the tensile surface, and it was possible to have steps of different depths and thus vary the mode mixture.

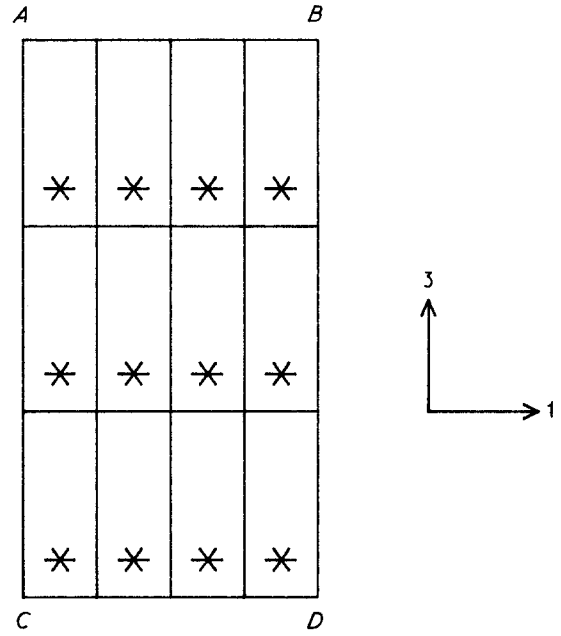

Figure 2 Original locations of specimens within plaque: (*) cracked end.

All tests were carried out using a universal testing machine operating at a constant crosshead speed; the operating speed was 2 mm min^{-1} for the Mode I tests and 0.5 mm min^{-1} for the other tests. Crack initiation was observed using an optical microscope focused on the crack-tip area on one side of the specimen. While several initiations were possible on a single specimen, as the crack progressed there was a tendency for the crack to become non-planar as a wavy crack front developed. Such a geometry is not amenable to analysis in two dimensions and so only the first initiations are used to characterize the material.

In the Mode I and Mode II tests, the notches were made by first sawing with a 0.4 mm slitting saw and then sharpening the resulting slit using a razor blade.

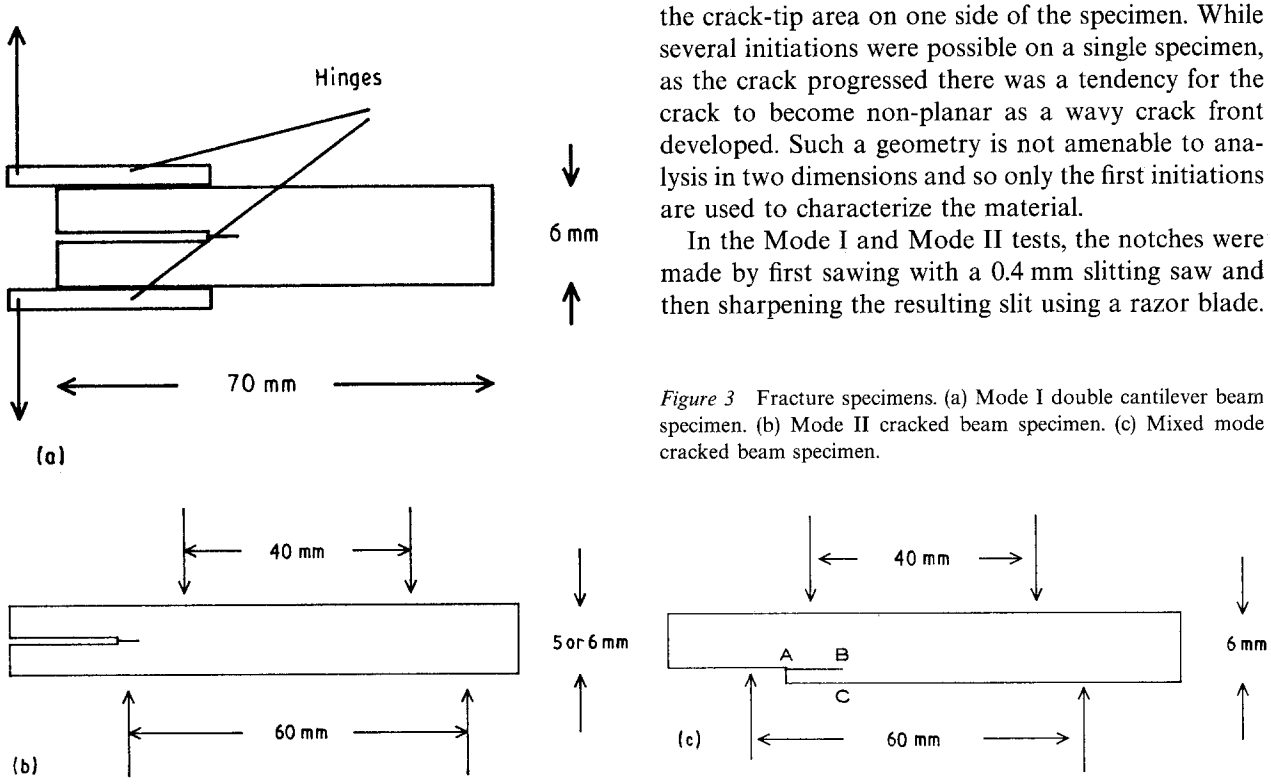

Figure 3 Fracture specimens. (a) Mode I double cantilever beam specimen. (b) Mode II cracked beam specimen. (c) Mixed mode cracked beam specimen.

In the mixed mode tests, razor blades were machined to give a chisel-shaped edge, and the flat surface of the blade slid along the step surface to form the notch AB starting from the corner at A. During this process, specimens were held in a special jig in which the blade could be inserted by turning a screw. In all cases, a crack was seen to open up ahead of the razor blade, so that the sharpness of the crack should not be critically dependent on the sharpness of the blade.

3. Analysis

3.1. Effects of inhomogeneity

For plane problems, the stress fields acting around crack tips are characterized as either opening mode or sliding mode (Modes I and II, respectively); a mixed or combined mode field can then be viewed as the algebraic sum of Mode I and Mode II fields. In experiments on homogeneous material, the mode of failure can be controlled by selecting an appropriate symmetry of loading of the specimen. However, when there is inhomogeneity in the vicinity of a crack tip, mixed mode loading is likely to result even when the specimen has a symmetry of the kind normally associated with loading in one mode only. As a result, the materials studied here can be expected to be subject to mixed mode loading in practice; for this reason, our experiments and analysis include combined mode behaviour.

The effect of inhomogeneity can be appreciated by consideration of the interfacial crack of Fig. 4; here, the crack grows along the interface of two materials of different elastic properties. If tension normal to the crack is applied to this system, the mismatch in lateral stress at the interface ensures that some shear stresses develop and that there is some Mode II loading of the crack tip; this is in contrast to the pure Mode I loading that would obtain in a homogeneous body. The case of a crack between dissimilar isotropic media has been discussed most recently by Rice [8], and some attention [9–12] has been paid to the problem when the materials are anisotropic. The interfacial crack presents special problems theoretically, in that conventional definitions of stress intensities K_I and K_{II} are not strictly applicable. However, in qualitative terms it resembles a crack which is not at an interface but close to one, and in this case K_I and K_{II} are well defined. In the experimental problems discussed here, it is not necessary to analyse truly interfacial flaws, and the cracks are considered to be growing in homogeneous regions of material but subject to a mixture of loading which may be influenced by the proximity of an interface.

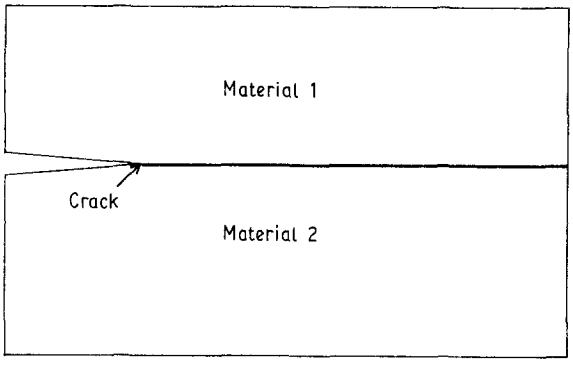

Figure 4 Interfacial crack.

The theoretical treatment must be applicable to inhomogeneous bodies. Finite-element analysis is a readily available method, and is used in such a way as to determine the relative proportions of Modes I and II and the relevant fracture parameters.

3.2. Evaluation of fracture parameters

In this section we describe the methods used to obtain two alternative characterizations of fracture behaviour. The crucial requirement is that, given a crack subject to mixed mode conditions, the proportions of the loading attributable to Modes I and II be calculated. This can be done either in terms of the stress intensities K_I and K_{II} or the strain energy release rates G_I and G_{II} [13]. When extracting these data via the finite element method, a major consideration is that the stress field near to the crack tip will be poorly modelled; therefore, the stress intensities, which are defined in terms of the near-tip stress field, cannot be determined directly from the calculated stresses. The determination of strain energy release rates is not subject to this problem, and they are therefore used as the basis for calculating the stress intensities as well as to provide a description of the fracture behaviour in their own right.

The method for calculating strain energy release rates proposed by Rybicki and Kanninen [14] is suitable only when using constant strain elements, and has been extended to higher order elements, such as those used here, by Raji [15]. However, both methods depend upon values of nodal forces near to the crack tip, and it was considered that the proximity of a material interface could jeopardize their reliability. The strategy finally adopted was to use virtual crack increments to determine strain energy release rates via global energy considerations, and to derive K_I and K_{II} from these quantities via the known relations of fracture mechanics.

When constant loads F_i are applied per unit thickness to points on a cracked body, and the crack extends a distance δc, each loaded point responds by moving a distance δv_i along the direction of F_i. For sufficiently small crack increments, δc, we may assume that the strain energy release rate, G, is given by

$$G = \frac{1}{2\delta c} \sum_i F_i \delta v_i \qquad (1)$$

where the force F_i is applied to the ith loaded point. The associated displacements of nodal points on the faces of the crack increment which would apply in a finite-element model is shown in Fig. 5a. The analysis is carried out initially with nodes either side of the crack face coupled, and the displacements of the loaded boundary nodes calculated; the crack is then extended by uncoupling the nodes and the procedure repeated to find the changes in displacement, δv_i. This

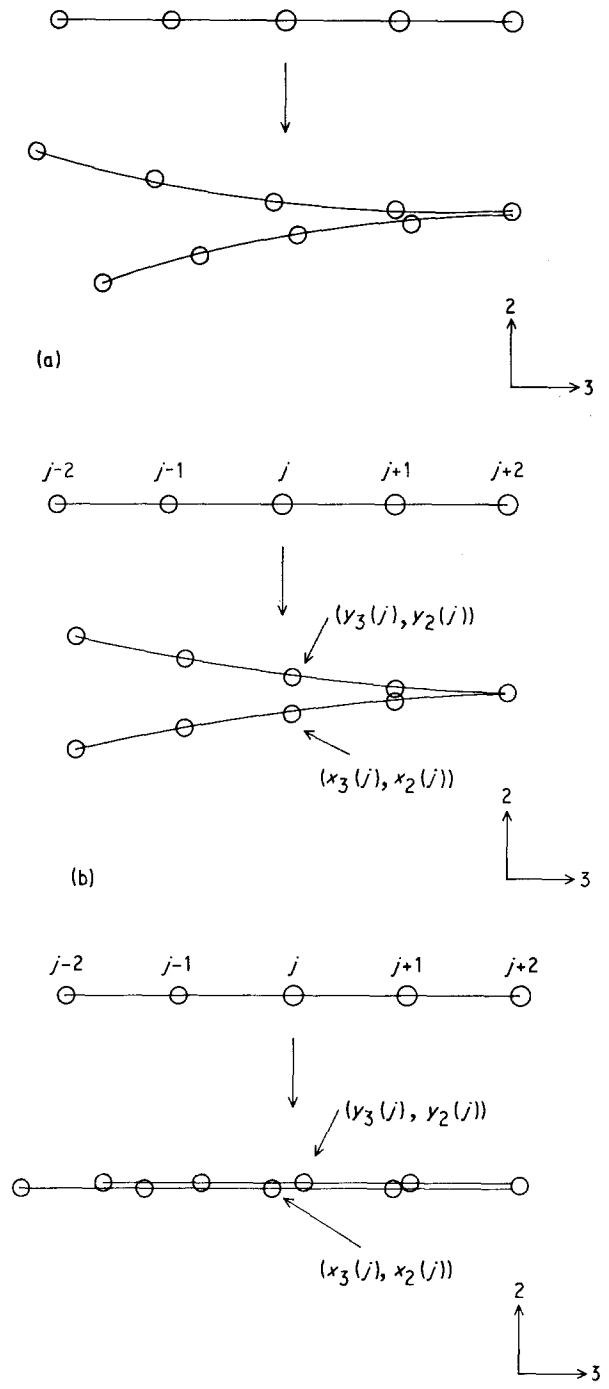

Figure 5 Finite-element modelling of crack increments in (a) mixed mode, (b) Mode I, and (c) Mode II.

gives the total strain energy release rate, G, where

$$G = G_I + G_{II} \tag{2}$$

G_I and G_{II} are defined as the strain energy release rates when the relative displacement of the crack faces after crack growth is restricted in the manner appropriate for the particular mode. In the case of Mode I, the restriction is such that no relative sliding of initially coincident nodes is allowed; this case is illustrated in Fig. 5b. If the positions of nodes after crack growth are given on the lower face by $\boldsymbol{x} = (x_3(j), x_2(j))$ and on the upper face by $\boldsymbol{y} = (y_3(j), y_2(j))$, where the nodes associated with the index j were coincident before crack growth, for the Mode I case, the restriction takes the form $x_3(j) = y_3(j)$ for each j, and the finite-element solution is subject to this constraint. Then G_I is calculated by applying the concept of Equation 1

$$G_I = \frac{1}{2\delta c}\sum_i F_i \delta v_i \Bigg|_{\substack{x_3(j)=y_3(j) \\ \text{for each node pair } j \\ \text{on crack increment}}} \tag{3}$$

Analogously, G_{II} is obtained by restricting the crack faces so that there is no crack opening: $x_2(j) = y_2(j)$ for each j. This is illustrated in Fig. 5c. G_{II} is then calculated as

$$G_{II} = \frac{1}{2\delta c}\sum_i F_i \delta v_i \Bigg|_{\substack{x_2(j)=y_2(j) \\ \text{for each node pair } j \\ \text{on crack increment}}} \tag{4}$$

G_I and G_{II} can be used to characterize mixed mode material behaviour. As an alternative, the stress intensities K_I and K_{II} may be used for this purpose. The experimental results may show that one or other of these interpretations is preferable, and so both will be implemented and their performances compared.

Two methods of deriving K_I and K_{II} are presented and used together to check consistency. In the first method, the stress intensities are directly related to G_I and G_{II}. For an orthotropic material with a crack extending collinearly along one of the planes of orthotropy, K_I and K_{II} are related to G_I and G_{II} by

$$K_I^2 = E_I G_I \tag{5a}$$

$$K_{II}^2 = E_{II} G_{II} \tag{5b}$$

where E_I and E_{II} are material parameters defined by Sih *et al.* [16]

$$1/E_I = (t_{22}t_{33}/2)^{1/2}[(t_{22}/t_{33})^{1/2} + (2t_{23} + t_{44})/2t_{33}]^{1/2} \tag{6a}$$

$$1/E_{II} = (t_{33}/2^{1/2})[(t_{22}/t_{33})^{1/2} + (2t_{23} + t_{44})/2t_{33}]^{1/2} \tag{6b}$$

Here plane strain conditions are assumed and the t_{ij} in Equations 6a and b are related to the compliances, s_{ij}, by

$$t_{ij} = s_{ij} - s_{i1}s_{j1}/s_{11} \qquad i,j = 2,3 \tag{6c}$$

In the second method, the stress intensities are obtained from the total strain energy release rates associated with crack increments in different directions. A minimum of two crack increments, with no restriction on the crack face deformations, gives sufficient information to derive K_I and K_{II}. For the collinear crack as shown in Fig. 5a, the total strain energy release rate, G, is related to K_I and K_{II} by

$$G = K_I^2/E_I + K_{II}^2/E_{II} \tag{7}$$

This is consistent with Equations 2 and 5. For a crack extending at an angle to its initial direction, the Modes I and II stress fields interact to give a further contribution to the strain energy release rate. For a crack extending at right angles to its initial direction, as depicted in Fig. 6, the strain energy release rate, G_n, is given by

$$G_n = AK_I^2 + BK_{II}^2 + CK_IK_{II} \tag{8}$$

This is an exact relation [17]. It is emphasized that,

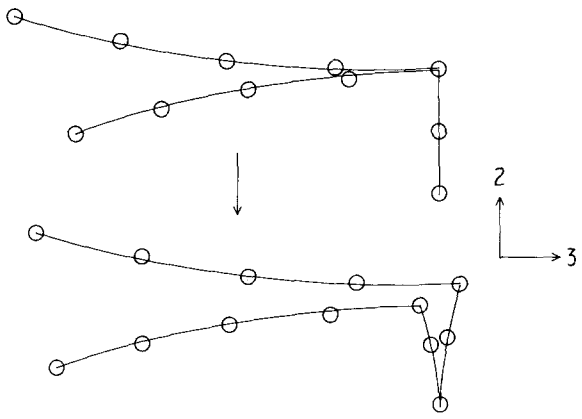

Figure 6 Crack increment normal to initial crack direction.

unlike all the other strain energy release rates, G_n is not associated with a crack path observed experimentally and is solely a computational device. The parameters A, B and C can be calculated numerically for a particular material by evaluating G_n for a range of values of K_I and K_{II}; finite-element analysis of suitably loaded centre-cracked plates has been used successfully for this purpose [18]. Using the appropriate compliances as given in Table I, plane strain values of A, B and C have been calculated using the method described previously [18]. Then, once G and G_n have been calculated using the virtual crack-extension method via Equation 1, there is sufficient information to solve Equations 7 and 8 to give K_I and K_{II}.

In summary, the method of calculating G_I and G_{II} and two alternative methods of calculating K_I and K_{II} are outlined above. Both methods of deriving the stress intensities were exploited and their consistency confirmed, as described in the next section; this assurance is particularly desirable in view of the inaccuracies which can be generated by an inappropriate choice of the length of crack increment, δc.

3.3. Finite element modelling

To apply the methods of the previous section to the experiments outlined in Section 2.2, finite-element models are required of the experimental specimens. The modelling was carried out using the package PAFEC under the assumption of linear elastic material behaviour. The models are two-dimensional and consist of eight-noded isoparametric elements with the ability to model orthotropic material behaviour. The specimens depicted in Fig. 3a–c are modelled by meshes shown, respectively, in Fig. 7a–c.

With one exception, the specimens were of thickness in the 2 direction corresponding to the full plaque thickness. Therefore, in the models, the material properties are everywhere as defined by the 'core' values of Table I except for the outer 0.3 mm thick layer of elements which are assigned the 'skin' values. The exception occurs in some of the Mode II specimens, where ~ 0.5 mm surface layers were peeled off before testing. In this case the models were as in Fig. 7b but with the outer element layers removed and the total thickness modified to 5 mm.

For each specimen there are two load points at which the forces F_1 and F_2 of Equations 1, 3 or 4 are applied. In all cases a range of crack lengths AB which spanned the range covered in the experiments was studied. In the Mode I tests of Figs 3a and 7a the effects of the hinges on the specimen behaviour were taken into account by including them in the finite-element model as strips of isotropic material having the properties of mild steel. These tests are symmetric about the line of the crack, and therefore only half the specimen need be modelled; the mesh of Fig. 7a was developed to enable the effects of off-centre cracks to be examined and for convenience its use was continued for the symmetrical cases. Cracks which deviated from the centre line by amounts comparable with those observed in the experiments were found not to have any significant effects. For the mixed mode tests of Figs 3c and 7c, the step depth BC was varied to accommodate those used experimentally $-$ 0.3, 1 and 3 mm. The mesh shown is for the 1 mm step; meshes for other step sizes are minor variations of this.

The modelling of the crack-tip region is common to all the meshes and is shown in Fig. 8. The collinear crack increment for obtaining G, G_I and G_{II} is DB. To establish that this increment gave convergent values of strain energy release rate, shorter increments along the

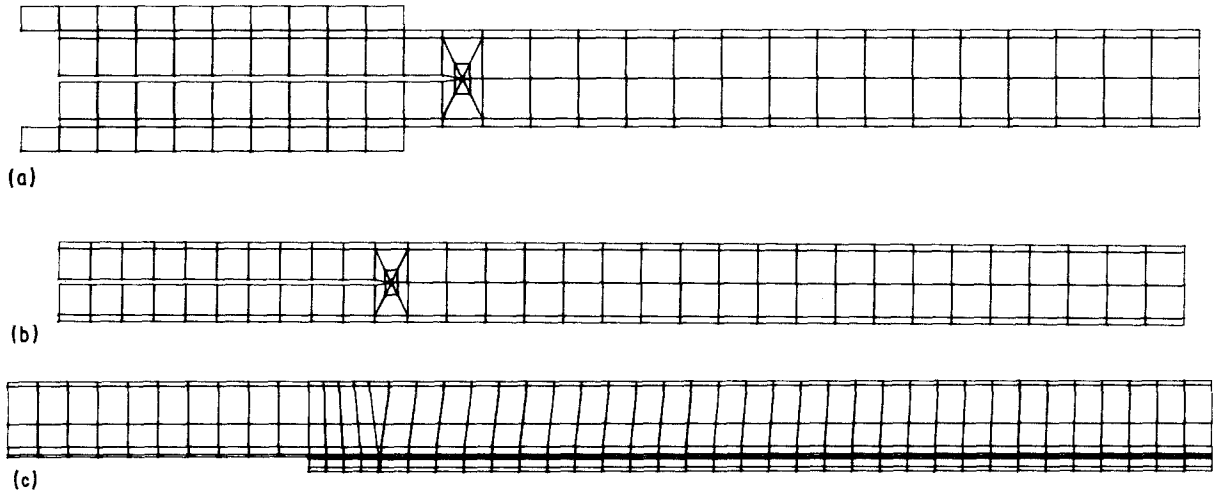

Figure 7 Finite-element meshes of (a) Mode I specimen of Fig. 3a, (b) Mode II specimen of Fig. 3b, and (c) mixed mode specimen of Fig. 3c.

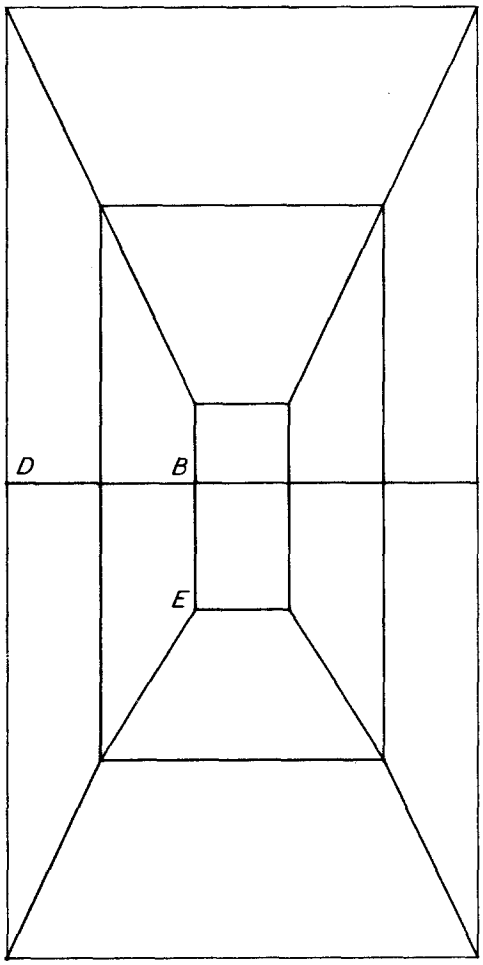

Figure 8 Elements in crack-tip area.

line *DB* were tried. The values so obtained were consistent with those obtained using the whole length DB, and confirmed the validity of the procedure. The increment along *BE* is used for evaluating G_n; the length *BE* can varied by changing the associated element lengths. It was found that the value of G_n was significantly dependent on the length *BE*. However, results for G_n consistent with the G_I and G_{II} values were obtained when *BE* was of similar length to *DB*. In this sense the two methods are consistent, but the use of the collinear crack increment and evaluation of G_I and G_{II} is the more reliable. The results of the experiments are interpreted using this method.

In the case of the model of the mixed mode specimen with the 0.3 mm deep step, the crack line *DB* is exactly 0.3 mm below the specimen surface and therefore in line with the interface between the skin and core material. However, a truly interfacial crack poses the theoretical difficulties outlined in Section 3.1 of the definition of K_I and K_{II}. Also, in the specimens, the skin–core interface is not as strictly defined as in the model; it is not perfectly plane and so some points on the crack front will be entirely in the skin and others entirely in the core. It is likely that for such a crack, initiation will be controlled by the points on the crack front which experience the most destructive stress field. The elastic properties of the elements immediately adjacent to the crack tip can be adjusted to give any of the three conditions: crack in skin material, crack in core material, and crack at the interface. The values of G_I and G_{II} were calculated for each of these conditions, and it was found that G_I did not vary, but that G_{II} varied so that it was least when the crack was in the skin material, but effectively equal for the other two conditions. Values of K_I and K_{II} were therefore calculated on the basis that the crack advanced into core material.

4. Results and discussion

4.1. Single mode testing

The results for the mode I double cantilever beam tests of Fig. 3a are given in Fig. 9 in the form of K_{Ic} plotted as a function of crack length. While there is an apparent trend of toughness decreasing with crack length, the genuineness of the dependence is doubtful owing to the scatter in the data. We therefore assume that the toughness can be estimated from a simple average. The mean value of K_{Ic} is then 1.50 ± 0.13 MN m$^{-3/2}$ (the range of the error is a 95% confidence interval). For a crack extending along the direction of orientation, toughnesses are found to be similar in value to those for the isotropic polymer; the value here is similar to that found for oriented polyethylene [19] when cracks propagate along the direction of orientation.

The results for the Mode II tests of Fig. 3b are plotted similarly as K_{IIc} in Fig. 10. There is no discernible crack-length dependence. For these tests, two sets of specimens were made with different degrees of inhomogeneity, by peeling off 0.5 mm skins from the surfaces of some of them. The two sets of toughness

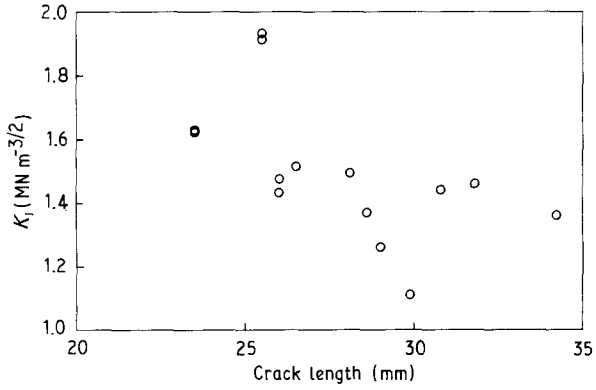

Figure 9 Results for Mode I fracture from double cantilever beam tests.

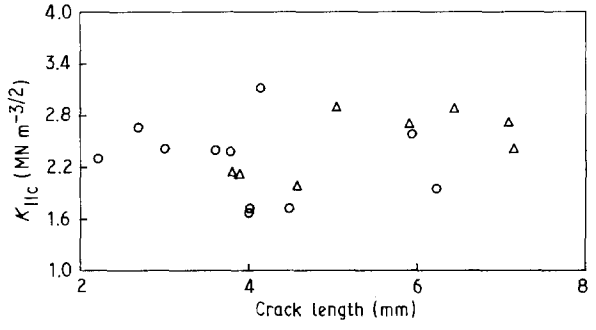

Figure 10 Results for mode II fracture from split beam tests. (○) Full thickness, (△) skins removed.

values so obtained were not significantly different at the 10% level; this gives some assurance of the overall validity of the method of analysis. The combined value of K_{IIc} is 2.36 ± 0.42 MN m$^{-3/2}$. In common with the fracture behaviour of isotropic polymers [20], polymer composites [21] and wood [22], the toughness in Mode II is significantly greater than that in Mode I. When expressed in terms of strain energy release rate, these results give $G_{Ic} = 0.57 \pm 0.1$ kJ m^{-2} and $G_{IIc} = 1.05 \pm 0.18$ kJ m^{-2}.

4.2. Mixed mode testing

The test geometry is that of Fig. 3c. The step depth BC was one of three values — 0.3, 1.0 and 3.0 mm. The results for the 3 mm steps were inconsistent with all the other tests. In particular, the combination of stress intensities required in the 3 mm step tests to initiate cracking (which we denote by $(K_I, K_{II})_c$) was on average such that $K_I > K_{Ic}$ and $K_{II} > K_{IIc}$, where K_{Ic} and K_{IIc} are the values obtained in single mode testing. The concept that the crack is driven by the combined action of the two modes leads directly to the expectation that $K_I < K_{Ic}$ and $K_{II} < K_{IIc}$. The results from the finite-element analyses showed that, at the observed failure loads, the stresses in the region of the specimens between the lower and upper rollers at the crack end was much higher for the 3 mm steps than for the shallower steps, the von Mises stress in the deeper step specimen being greater by a factor of three, and at some points considerably higher than the compressive yield stress of 80 MPa. It seems likely that the 3 mm step specimen will yield in a complex way and that its behaviour is not easily quantifiable. Therefore, we exclude these results from the discussion.

The remaining mixed mode results for the 0.3 and 1.0 mm steps are shown, together with the single mode results, in Fig. 11, where each data point corresponds to a fracture initiation. The average values are plotted similarly in Fig. 12.

4.3. Fracture criteria

We now seek to consider whether it is possible to represent the data for opening mode, sliding mode and mixed mode fracture by a simple fracture criterion based on either stress intensities or strain energy

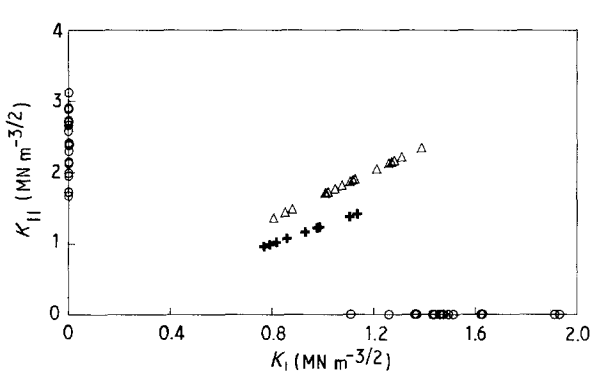

Figure 11 Summary of all single and mixed mode tests. (●) 3 mm deep slit, (△) 0.3 mm deep step, (+) 1 mm deep step.

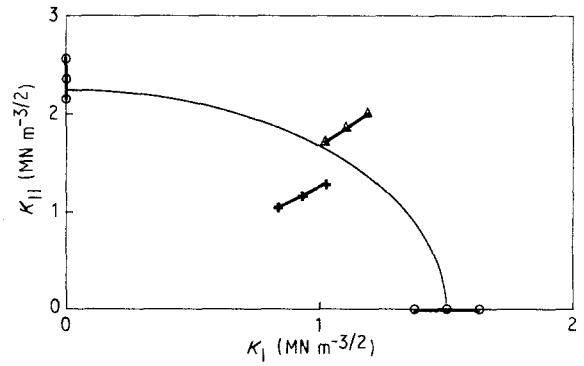

Figure 12 Average values showing 95% confidence interval error bars and fitted curve from Equation 9. (○) 3 mm deep slit, (△) 0.3 mm deep step, (+) 1 mm deep step.

release rates. The idea is that failure can be predicted for any combination of K_I and K_{II} or G_I and G_{II} from a single equation involving K_{Ic} and K_{IIc} or G_{Ic} and G_{IIc}, respectively. This is analogous to a yield criterion which governs yielding when material is subject to combined stresses.

The relation

$$(K_I/K_{Ic})^2 + (K_{II}/K_{IIc})^2 = 1 \qquad (9)$$

has been proposed as an empirical fracture criterion by Wu [22]. This equation has been fitted to the average values and the corresponding curve is plotted on Fig. 12. The values of K_{Ic} and K_{IIc} obtained from the fitting process are, respectively, 1.50 and 2.25 MN m$^{-3/2}$, not significantly different from the results for the single mode tests. The curve of Equation 9 matches the observations adequately.

The equivalent results in terms of G_I and G_{II} are plotted an average values in Fig. 13. For strain energy release rate, a failure criterion equivalent to Equation 9 is

$$G_I/G_{Ic} + G_{II}/G_{IIc} = 1 \qquad (10)$$

This can be obtained via the use of Equations 5a and b in Equation 9. The fitted line from Equation 10 is shown in Fig. 13. Values of G_{Ic} and G_{Ic} obtained via the fitting procedure are, respectively, 0.57 and 0.95 kJ m^{-2}, consistent with the single mode results. The two Equations 9 and 10 given a similar quality of fit to the data, suggesting that fracture can be viewed

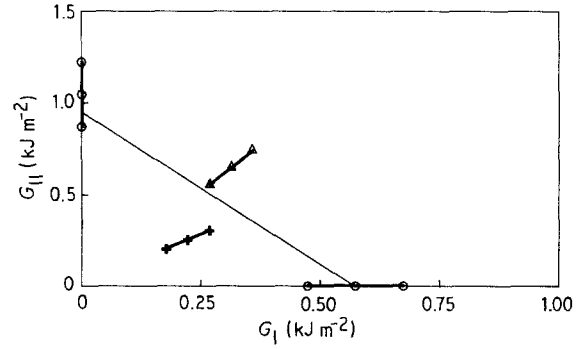

Figure 13 Average values in terms of strain energy release rates, showing 95% confidence interval error bars and fitted line from Equation 10. (a) 3 mm deep slit, (△) 0.3 mm deep step, (+) 1 mm deep step.

as being controlled by stress intensity or strain energy release rate with equal validity.

5. Conclusions

1. Fracture of liquid-crystal polymer has been studied in the case of cracks propagating in the plane of injection-moulded plaques, using both single mode and mixed mode testing. Results have been interpreted in terms of both strain energy release rate and stress intensity, and it is found that both $K_{Ic} < K_{IIc}$ and $G_{Ic} < G_{IIc}$.

2. Simple fracture criteria in terms of K_I and K_{II} or G_I and G_{II} are effective in predicting the initiation of a crack in the plane of the moulding. Cracks at different depths within the moulding and therefore in material with different elastic properties can be described by the same criterion.

Acknowledgement

This work is the result of a collaborative project with ICI, Wilton, UK. We acknowledge ICI for its financial support.

References

1. H. THAPAR and M. J. BEVIS, *J. Mater. Sci. Lett.*, **2** (1983) 733.
2. T. WENG, A. HILTNER and E. BAER, *J. Mater. Sci.* **21** (1986) 744.
3. H. THAPAR and M. J. BEVIS, *Plastics Rubber Process. Applic.* **12** (1989) 39.
4. D. J. BLUNDELL, R. A. CHIVERS, A. D. CURSON, J. C. LOVE and W. A. MacDONALD, *Polymer* **29** (1988) 1459.
5. L. C. SAWYER and M. JAFFE, *J. Mater. Sci.* **21** (1986) 1897.
6. Z. OPHIR and Y. IDE, *Polym. Engng Sci.* **23** (1983) 792.
7. J. SWEENEY, B. BREW, R. A. DUCKETT and I. M. WARD, *Polymer*, Submitted.
8. J. R. RICE, *J. Appl. Mech.* **55** (1988) 98.
9. D. L. CLEMENTS, *Int. J. Engng Sci.* **9** (1971) 257.
10. G. R. MILLER, *ibid.* **27** (1989) 667.
11. C. T. SUN and M. G. MANOHARAN, *J. Compos. Mater.* **23** (1989) 460.
12. Z. SUO, *Proc. R. Soc. London* **A427** (1990) 331.
13. J. G. WILLIAMS, *Int. J. Fract.* **36** (1988) 98.
14. E. F. RYBICKI and M. F. KANNINEN, *Engng Fract. Mech.* **9** (1977) 931.
15. R. S. RAJI, *ibid.* **28** (1987) 251.
16. G. C. SIH, P. C. PARIS and G. R. IRWIN, *Int. J. Fract.* **1** (1965) 189.
17. F. ERDOGAN and G. C. SIH, *J. Basic Engng Trans. ASME D* **85** (1963) 519.
18. J. SWEENEY, *Int. J. Fract.* **47** (1991) 69.
19. J. SWEENEY, R. A. DUCKETT and I. M. WARD, *Proc. R. Soc. London* **A420** (1988) 53.
20. J. G. WILLIAMS, "Fracture Mechanics of Polymers" (Ellis Horwood, Chichester, 1984) p. 75.
21. E. F. RYBICKI, T. D. HERNANDEZ Jr, J. E. DEIBLER, R. C. KNIGHT and S. S. VINSON, *J. Compos. Mater.* **21** (1987) 105.
22. E. M. WU, *J. Appl. Mech.* **34** (1967) 967.

Received 14 November
and accepted 27 November 1991